Cellular/Molecular

Cellular Dynamics of Cholinergically Induced α (8–13 Hz) Rhythms in Sensory Thalamic Nuclei *In Vitro*

Magor L. Lörincz, Vincenzo Crunelli, and Stuart W. Hughes
School of Biosciences, Cardiff University, Cardiff CF10 3US, United Kingdom

Although EEG α (8–13 Hz) rhythms are traditionally thought to reflect an "idling" brain state, they are also linked to several important aspects of cognition, perception, and memory. Here we show that reactivating cholinergic input, a key component in normal cognition and memory operations, in slices of the cat primary visual and somatosensory thalamus, produces robust α rhythms. These rhythms rely on activation of muscarinic receptors and are primarily coordinated by activity in the recently discovered, gap junction-coupled subnetwork of high-threshold (HT) bursting thalamocortical neurons. By performing extracellular field recordings in combination with intracellular recordings of these cells, we show that (1) the coupling of HT bursting cells is sparse, with individual neurons typically receiving discernable network input from one or very few additional cells, (2) the phase of oscillatory activity at which these cells prefer to fire is readily modifiable and determined by a combination of network input, intrinsic properties and membrane polarization, and (3) single HT bursting neurons can potently influence the local network state. These results substantially extend the known effects of cholinergic activation on the thalamus and, in combination with previous studies, show that sensory thalamic nuclei possess powerful and dynamically reconfigurable mechanisms for generating synchronized α activity that can be engaged by both descending and ascending arousal systems.

Key words: **acetylcholine; lateral geniculate nucleus; electrical synapses; gap junctions; oscillations; EEG; cognition; memory**

Introduction

α Rhythms are EEG oscillations at ~8–13 Hz that are most apparent during relaxed wakefulness (Berger, 1929). The two best characterized α rhythms are the classical occipital rhythm of the visual cortex (Berger, 1929; Adrian and Matthews, 1934; Adrian and Yamagiwa, 1935) and the μ rhythm of the sensorimotor cortex (Pfurtscheller et al., 1997; Pineda, 2005). Although these rhythms are traditionally thought to reflect an "idling" of primary cortical areas, a large body of evidence suggests that they also play important roles in cognitive processes and sensory perception (VanRullen and Koch, 2003). For example, α rhythm frequency displays a consistent relationship with both reaction time (Surwillo, 1961) and the maximal interstimulus interval for simultaneity judgment (Kristofferson, 1967). Stereotyped changes in α rhythm power are also closely associated with certain semantic memory tasks (Klimesch, 1999).

Studies in both humans and animals have consistently identified the thalamus as a key site for α rhythm generation (summarized in Hughes and Crunelli, 2005). In animal studies, a combination of chronic electrophysiological recording and appropriately targeted lesions have directly implicated the lateral geniculate nucleus (LGN) (visual thalamus) and ventrobasal complex (VB) (somatosensory thalamus) in the production of analogs of the occipital α rhythm (Lopes da Silva et al., 1973a,b; Chatila et al., 1992, 1993) and μ rhythm (Rougeul-Buser et al., 1975; Bouyer et al., 1982, 1983; Rougeul-Buser and Buser, 1997), respectively. Recently, we highlighted a subset of thalamocortical (TC) neurons in the cat LGN that can exhibit a novel type of intrinsic burst firing at α frequencies, termed high-threshold (HT) bursting (Hughes et al., 2002, 2004). This activity was unmasked by activation of the metabotropic glutamate receptors (mGluRs) that are postsynaptic to corticothalamic fibers (i.e., mGluR1a) (McCormick and von Krosigk, 1992; Godwin et al., 1996a,b) and could be synchronized by gap junctions (GJs) to form a local α rhythm generator (Hughes et al., 2004).

In addition to the considerable mGluR1a-mediated innervation provided by cortical feedback, thalamic relay nuclei also receive a substantial cholinergic input from the brainstem (de Lima et al., 1985). Furthermore, because the muscarinic receptors that are targeted by this input are coupled to similar postsynaptic targets on TC neurons to mGluR1a (McCormick and Prince, 1987; McCormick and von Krosigk, 1992), we hypothesized that muscarinic activation might also lead to synchronized α oscillations. Interestingly, although the effects of cholinergic activation on individual thalamic neurons have been extensively investigated (McCormick and Prince, 1987; McCormick, 1992; Zhan et al., 2000), its influence on thalamic network activity is poorly understood. In this study, we therefore examined the consequences of cholinergic activation for regional network activity in slices of the cat LGN and VB maintained *in vitro*. We demonstrate that, in both nuclei, cholinergic input acting via muscarinic receptors does indeed induce synchronized α oscillations that are

Received Sept. 30, 2007; revised Nov. 16, 2007; accepted Nov. 21, 2007.

This work was supported by Wellcome Trust Grants 71436, 78403, and 78311 (V.C., S.W.H.). We thank Dr. David. W. Cope for helpful comments on a previous version of this study.

Correspondence should be addressed to Stuart W. Hughes, School of Biosciences, Cardiff University, Museum Avenue, Cardiff CF10 3US, UK. E-mail: hughessw@cardiff.ac.uk.

DOI:10.1523/JNEUROSCI.4468-07.2008

 0270-6474/08/280660-12$15.00/0

shaped by a GJ-coupled subnetwork of HT bursting TC neurons. By examining the suprathreshold and subthreshold activity of these neurons during cholinergically induced α rhythms, we highlight a number of fundamental aspects of their oscillation-related cellular dynamics.

Materials and Methods

All procedures were performed in accordance with local ethical committee guidelines and the United Kingdom Animals (Scientific Procedure) Act, 1986. All efforts were made to minimize the suffering and number of animals used in each experiment.

In vitro *slice preparation and maintenance.* Young adult cats (1–1.5 kg) were deeply anesthetized with a mixture of O_2 and NO_2 (2:1) and 2.5% isoflurane, a wide craniotomy was performed, and the brain was removed. Sagittal slices (450–500 μm) of the LGN or VB were prepared and maintained as described previously (Hughes et al., 2002, 2004; Blethyn et al., 2006). For recording, slices were perfused with a warmed (35 ± 1°C) continuously oxygenated (95% O_2, 5% CO_2) artificial CSF (ACSF) containing the following (in mM): 134 NaCl, 2 KCl, 1.25 KH_2PO_4, 1 $MgSO_4$, 2 $CaCl_2$, 16 $NaHCO_3$, and 10 glucose. Sources of drugs were as follows: DL-2-amino-5-phosphonovaleric acid (NMDA receptor antagonist), [*S*-(*R**,*R**)]-[3-[[1-(3,4-dichlorophenyl)ethyl]amino]-2-hydroxypropyl]-(cyclohexylmethyl)phosphinic acid (CGP54626) ($GABA_B$ receptor antagonist), 6-cyano-7-nitroquinoxaline-2,3-dione (CNQX) (AMPA/kainate receptor antagonist), 1,1-dimethyl-4-diphenylacetoxypiperidinium iodide (4-DAMP) (M_3 receptor antagonist), 8-methyl-8azabicyclo-3-*endo*[3,2,1]oct-3-yl-1,4-dihydro-2-oxo-3(2*H*)-quinazolinecarboxylic acid ester hydrochloride (DAU-5884) (M_3 receptor antagonist), 6-imino-3-(4-methoxyphenyl)-1(6*H*)-pyridazinebutanoic acid hydrobromide (SR95531) ($GABA_A$ receptor antagonist), 4,9-dihydro-3-methyl-4-[(4-methyl-1-piperazinyl)acetyl]-10*H*-thieno[3,4-b][1,5]benzodiazepin-10-one dihydrochloride [telenzepine (Tzp)] (M_1 receptor antagonist) from Tocris Bioscience (Bristol, UK), carbamylcholine chloride [carbachol (Cch)] (nonselective cholinergic agonist), carbenoxolone (CBX) (GJ blocker), 18β-glycyrrhetinic acid (18β-GA) (GJ blocker), glycyrrhizic acid (GZA) (glycyrrhetinic acid derivative that is inactive as a GJ blocker), and 5,11-dihydro-11-([4-methyl-piperazin]acetyl)-6*H*-pyriso(2,3-b)(1,4)benzodiazepine-6-one [pirenzipine (Pzp)] (M_1/M_3 receptor antagonist) were obtained from Sigma (Poole, UK). All drugs were dissolved in ACSF except 4-DAMP, 18β-GA, and GZA, which were dissolved in DMSO such that the total final volume of DMSO did not exceed 0.1%.

In vitro *electrophysiology.* Extracellular recordings were performed using glass pipettes filled with 0.5 M NaCl (resistance, 1–5 MΩ) connected to a Neurolog 104 differential amplifier (Digitimer, Welwyn Garden City, UK). Field and unit activities were simultaneously recorded through the same electrode by bandpass filtering at 2–15 Hz and 0.2–20 kHz, respectively. Multisite extracellular recordings were performed with linear arrays (Frederick Haer Company, Bowdoinham, ME) connected to a multichannel differential amplifier (Plexon, Dallas, TX). Independently mounted intracellular recordings, using the current-clamp technique, were performed with standard-wall glass microelectrodes filled with 1 M potassium acetate (resistance, 80–120 MΩ) and, in some cases, 2% biocytin or Neurobiotin and connected to an Axoclamp-2A amplifier (Molecular Devices, Sunnyvale, CA) operating in bridge mode. All recordings in the LGN were obtained from lamina A or A1 (Rougeul-Buser and Buser, 1997; Hughes and Crunelli, 2005), whereas all VB recordings were obtained from the ventral posterolateral nucleus (Bouyer et al., 1982, 1983; Rougeul-Buser and Buser, 1997). Impaled cells were identified as TC neurons using established criteria (Pirchio et al., 1997; Turner et al., 1997). Voltage and current records were digitally acquired and processed using pClamp 9 (Molecular Devices).

In vitro *data analysis.* The apparent input resistance (R_N) was estimated from voltage responses evoked at −60 mV by small (20–50 pA) hyperpolarizing current steps. Phase values of neuronal firing were analyzed by circular statistical methods using Oriana 2.0 software (Kovach Computing Services, Anglesey, UK). Quoted phase values are the circular means of the phases at which there was an oscillation-related peak in firing. Significant non-uniformity in the phase of firing relative to the

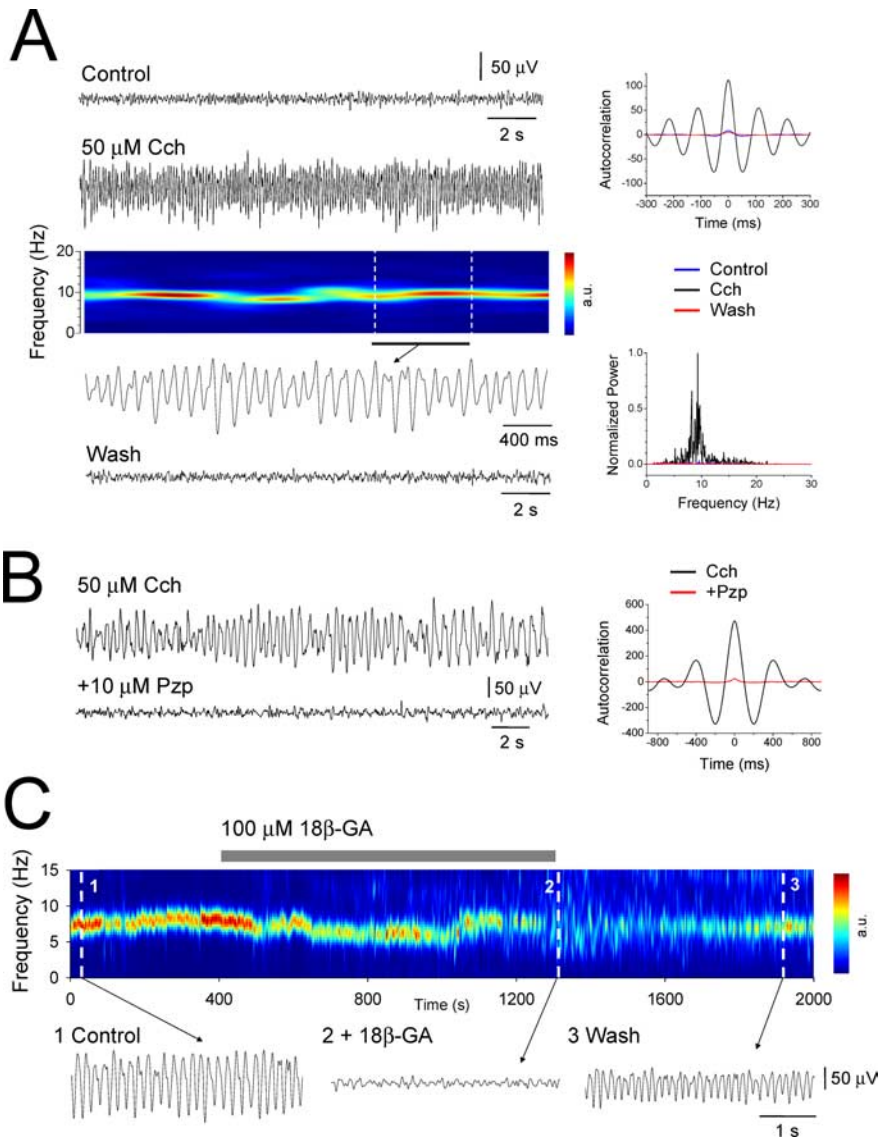

Figure 1. Muscarinic receptor activation elicits LFOs at α frequencies in slices of the cat LGN and VB that require intact GJ-mediated communication. ***A***, LGN extracellular field recording *in vitro* exhibiting α oscillations after 50 μM Cch application. The corresponding spectrogram is shown below (a.u., arbitrary units). The underlined section is further expanded below. The autocorrelation functions and power spectra pertaining to the Control, Cch, and Wash scenarios are shown on the right. ***B***, Cch-induced LFOs are abolished by the M_1/M_3 receptor antagonist Pzp. The corresponding autocorrelation functions are shown on the right. ***C***, Spectrogram showing a reversible disruption of Cch-induced α activity by the GJ-blocker 18β-GA. Raw traces are shown below as indicated.

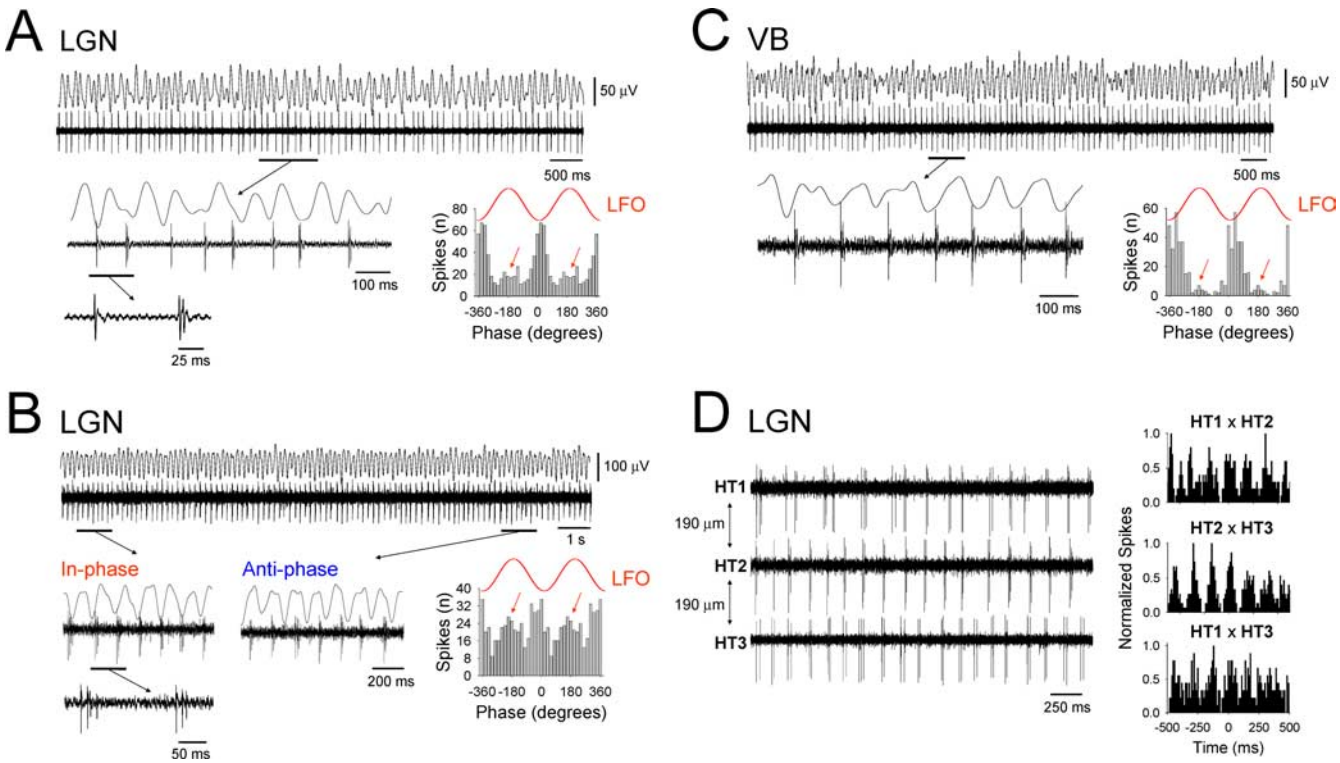

Figure 2. Cholinergically induced α rhythms are correlated with phase-shifting and synchronized HT bursting in TC neurons. ***A***, Simultaneous field and unit recording from the LGN slice preparation during ongoing Cch-induced α activity. The underlined section is enlarged below and shows the presence of HT bursts intermingled with single spikes (see the additional underlined section that is further enlarged below) (compare with Figs. 3*B2*, 4*B*). The corresponding spike timing histogram to the right illustrates that the majority of spikes occur close to the negative peak of the LFO. However, a small cluster of spikes also occur in an antiphase relationship (red arrows). ***B***, Additional example of a simultaneous field and unit recording from the LGN *in vitro*. Again, the underlined sections are enlarged below and reveal an HT bursting TC neuron that extensively shifts between periods of in-phase (1) and antiphase (2) firing with respect to the negative peak of the LFO (compare with Fig. 7*A*). Again, this phase-shifting is patently illustrated by the spike timing histogram to the right, which possesses two clear peaks. ***C***, LFOs in the VB *in vitro* are also associated with phase-shifting HT burst activity in individual TC neurons. In this case, HT bursting is manifested as rhythmic spike doublets (see underlined and enlarged section) (compare with Figs. 4*A*, 5*A*). ***D***, Three distinct HT bursting cells recorded in the presence of 50 μM Cch using a linear array of three independent electrodes, each separated by 190 μm. The corresponding cross-correlograms are shown on the right and reveal varying degrees of synchrony between the three cells. In this and all the following figures, the red traces labeled LFO are for references purposes only. Unless otherwise stated, 50 μM Cch was present in each of the experiments depicted in this and all subsequent figures.

ongoing local field oscillation (LFO) was tested for with Rao's spacing test ($p < 0.05$). This test calculates the probability of the null hypothesis that the data are distributed in a uniform manner. In all other cases, statistical significance was assessed using Student's *t* test. Absolute spike and spikelet times were determined using a straightforward visually determined threshold or peak detection approach, respectively. Typically, to construct a spike timing histogram, the times of at least 400 (for HT bursting cells) or 200 (for tonic firing cells) consecutive spikes were determined relative to the nearest negative peaks of the LFO using custom-written transform routines in SigmaPlot 9 (Systat, Hounslow, UK). These times were subsequently assigned a given phase between these peaks (i.e., between 0° and 360°) and then binned at 20° or 24° for HT bursting cells and 36° for tonic firing cells. For clarity, and to afford a sense of rhythmicity, these data were repeated over an additional full cycle of the oscillation (−360° to 0°) to produce the final plot (Klausberger et al., 2003, 2004; Hajos et al., 2004). For assessing the effect of firing in individual neurons on the amplitude of LFOs (see Fig. 10), neurons were allowed to fire spontaneously for at least 20 s. In some cases, neurons were permitted to fire for a longer period. However, this never resulted in an additional enhancement of the LFO because the full effect of individual neuron firing was always achieved within the first 20 s. Spectrogram plots were created using Neuroexplorer (Nex Technologies, Littleton, MA). All auto-correlation, cross-correlation, and power spectra plots were produced with OriginPro 7.5 (OriginLab, Northampton, MA). All quantitative data are expressed as mean ± SEM.

Results

Activation of muscarinic acetylcholine (ACh) receptors elicits population oscillations at α frequencies in slices of the cat LGN and VB that rely on GJs

In control conditions, extracellular field recordings obtained from slices of the cat LGN ($n = 52$) and VB ($n = 30$) exhibited a lack of spontaneous activity (Fig. 1*A*). However, application of the cholinergic agonist Cch (50 μM) reversibly induced robust LFOs in the α frequency band (mean frequency, 7.9 ± 0.3 Hz; mean peak-to-peak amplitude, 149.5 ± 12.4 μV; $n = 40$) (Fig. 1*A*) (see also Figs. 2, 6–10). These LFOs were persistent for the duration of Cch application and could often remain stable and unaltered for several hours. No significant differences were observed in either the mean frequency (LGN, 7.8 ± 0.4 Hz, $n = 28$; VB, 8.1 ± 0.5 Hz, $n = 12$; $p > 0.5$) or peak-to-peak amplitude (LGN, 154.3 ± 15.3 μV, $n = 28$; VB, 138.3 ± 22.1 μV, $n = 12$; $p > 0.5$) of LFOs between the LGN and VB. Application of lower concentration of Cch (25 μM) led to oscillations with both a reduced frequency (4.4 ± 0.4 Hz; $n = 8$) and lower mean peak-to-peak amplitude (52.0 ± 11.7 μV; $n = 8$). In both nuclei, the effect of Cch in bringing about LFOs was through muscarinic receptors because application of Pzp (1–10 μM) abolished all rhythmic activity (Fig. 1*B*). Because at low micromolar concentrations Pzp can block both muscarinic type 1 (M_1) and type 3

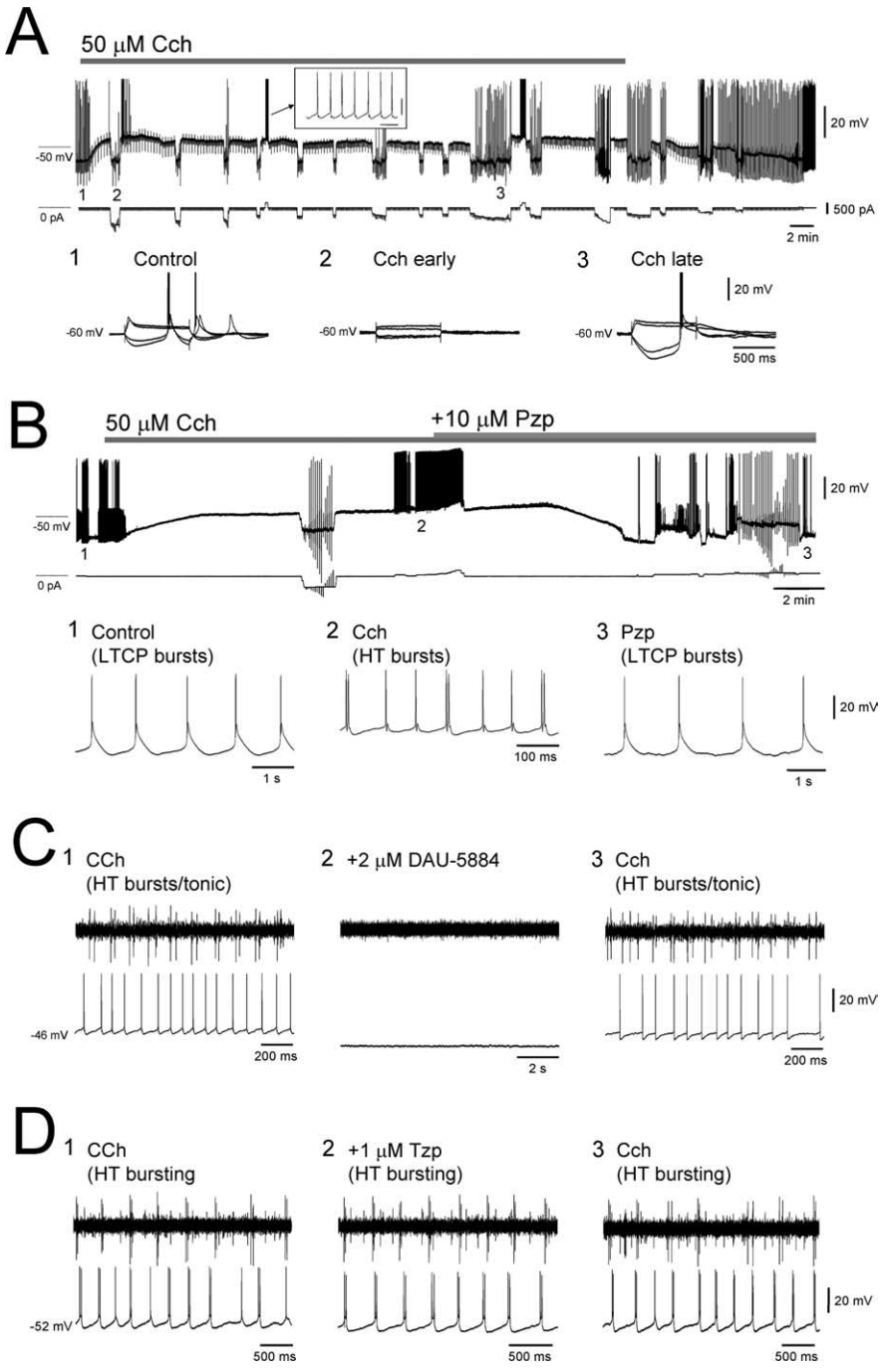

Figure 3. Basic effects of Cch on TC neurons *in vitro* assessed with intracellular recordings. ***A***, Application of 50 μM Cch to an LGN TC neuron *in vitro* causes a rapid depolarization that is initially associated with a profound reduction in input resistance R_N (***2***) but later with an increase in R_N (***3***). In this cell, the depolarization brought about by Cch shifts the cell to just below the threshold for tonic firing (see inset). ***B***, Example of an LGN TC neuron in which Cch application leads to a change from LTCP-mediated bursting (***1***) to HT bursting (***2***) and the reversal of this situation by Pzp (10 μM) (***3***). ***C***, Left, Simultaneous extracellular and intracellular recordings of an HT bursting TC neuron and a tonic firing cell, respectively. Middle, Application of 2 μM DAU-5884 abolished both types of activity and hyperpolarizes the tonic firing cell. Right, Washout of DAU-5884 leads to a reinstatement of both HT bursting and tonic firing. ***D***, Left, Simultaneous extracellular and intracellular recordings of two distinct HT bursting cells. Middle, Application of Tzp fails to affect either recording. Right, Activity is also unchanged after washout of Tzp.

(M_3) receptors (Zhu and Uhlrich, 1998; Lawrence et al., 2006a) and because immunohistochemical studies indicate a lack of M_1 receptors in the cat LGN (Plummer et al., 1999), we also examined the effects of the M_1 receptor preferring antagonist Tzp and the M_3 receptor preferring antagonist 4-DAMP. Tzp, applied at 1 μM, failed to inhibit cholinergically induced α oscillations ($n = 5$). Conversely, 4-DAMP (1 μM) consistently abolished α activity ($n = 5$) (supplemental Fig. 1*A*, available at www.jneurosci.org as supplemental material), suggesting that the effects of Cch in bringing about rhythmic α activity are most likely to be mediated mainly through M_3 receptors.

Cholinergically induced α oscillations were resistant to the application of blockers of ionotropic glutamate, $GABA_A$ and $GABA_B$ receptors (CNQX, 10 μM; APV, 50 μM; SR95531, 20 μM; CGP54626, 20 μM; $n = 10$) but were reversibly abolished by the GJ blockers CBX (100 μM) ($n = 4$) and 18β-GA (100 μM) ($n = 3$) (Fig. 1*C*) (Davidson and Baumgarten, 1988). Importantly, however, the glycyrrhetinic acid derivative that is inactive as a gap junction blocker, GZA (100 μM), failed to inhibit Cch-induced α activity ($n = 3$).

Cholinergically induced α rhythms are correlated with HT bursting in TC neurons

To assess the neuronal activity associated with cholinergically induced α oscillations, we obtained simultaneous extracellular field and single-unit recordings of TC neurons from the LGN and VB slice preparations. In control conditions, TC neurons were identified by the presence of sporadic or rhythmic (~1–2 Hz) low-threshold Ca^{2+} potential (LTCP)-mediated bursts (Leresche et al., 1991). After Cch (50 μM) application and the instigation of LFOs, the firing of theses neurons was reversibly altered in one of three ways: (1) neurons became quiescent ($n = 14$ of 82; 17%), (2) firing was transformed from LTCP-mediated bursting to single spike activity (mean frequency, 14.9 ± 1.2 Hz; $n = 40$ of 82; 49%) (data not illustrated) (McCormick and Prince, 1987; McCormick, 1992), or (3) firing was transformed from LTCP-mediated bursting to rhythmic HT bursting (8.3 ± 0.5 Hz; $n = 28$ of 82; 34%) (Fig. 2*A–C*) (Hughes et al., 2002, 2004). In all cells, HT bursts were of short duration, consisting of only two to four spikes [spikes per burst, 2.3 ± 1.1; interspike interval (ISI), 10.6 ± 0.6 ms; $n = 80$ bursts], which were typically intermingled with single spikes (Fig. 2*A*). In all cases, application of Pzp (1–10 μM) abolished HT burst generation so that neurons reverted to either intermittent or rhythmic LTCP-mediated bursting ($n = 12$). In agreement with field oscillation recordings, HT bursting was also abolished by the M_3 receptor preferring antagonists 4-DAMP (1–2 μM) ($n = 6$) and DAU-5884 (1–2 μM) ($n = 4$) but not by the M_1 receptor preferring antagonist Tzp when applied at 1 μM (control, 6.6 ± 1.6 Hz; Tzp, 6.2 ± 1.6 Hz; $n = 6$; $p > 0.5$) (Fig. 3*C*,*D*) (supplemental Fig. 1*B*, available at www.jneurosci.org as supple-

mental material). However, application of a higher concentration of Tzp (5 μM) reversibly blocked HT bursting ($n = 3$). When applied at ≤500 nM, neither 4-DAMP, DAU-5884, nor Tzp had an appreciable effect ($n = 3$ for each; data not illustrated). These results also implied a primary role for M_3 receptors in bringing about rhythmic activity. No significant differences were found in any of the properties of HT bursts (i.e., mean interburst frequency, spikes per burst, and ISIs) between neurons in the LGN and VB ($p > 0.5$).

The firing of all HT bursting neurons was significantly correlated to the LFO ($p < 0.05$, Rao's test), with the majority of spikes occurring close to the negative peak (9.5 ± 2.5°; $n = 28$) (Fig. 2*A–C*). However, in most cells, a substantial cluster of spikes also occurred in an antiphase relationship with the negative LFO peak (177.6 ± 3.5°; $n = 20$ of 28; 71%), indicating a dynamic switching in the phase at which these neurons prefer to fire (Fig. 2*A–C*, red arrows). This close association of HT bursting TC neurons with ongoing α oscillations clearly indicates that the activity of these cells is correlated. Indeed, as direct evidence of this, simultaneous recordings of distinct HT bursting neurons with independent extracellular electrodes mounted on a linear array often revealed clearly synchronous activity ($n = 8$) (Figs. 2*D*, 3*D*).

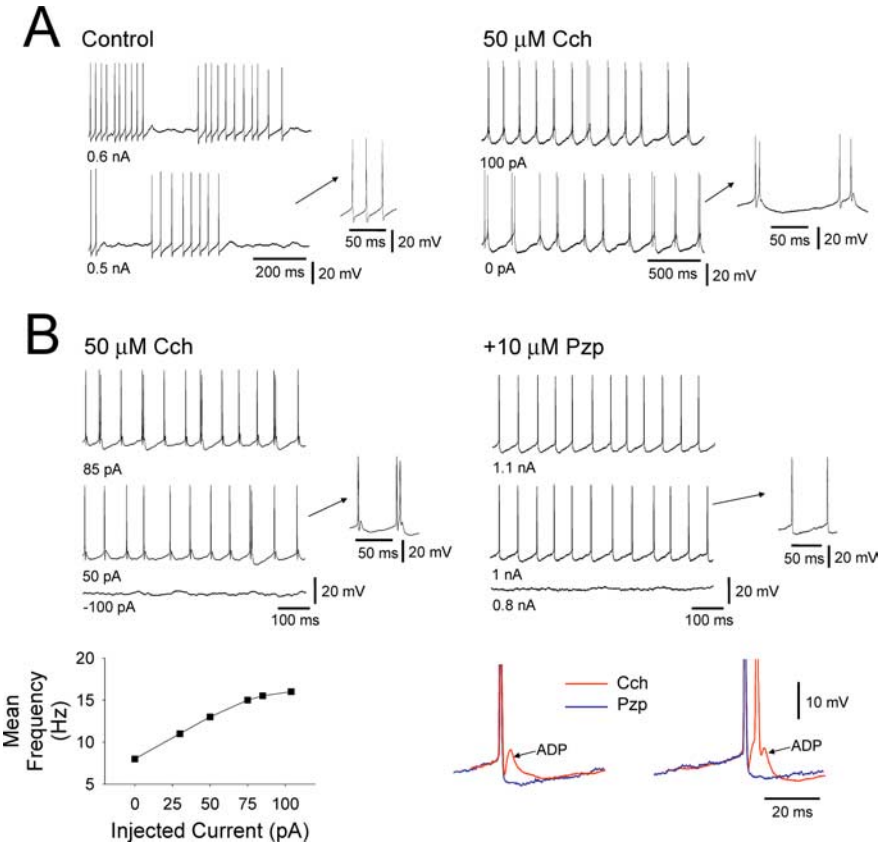

Figure 4. Properties Cch-induced HT bursting in TC neurons. ***A***, Comparison of the tonic firing that occurs in control conditions (left traces) with the HT bursting that is induced by Cch in an LGN TC neuron *in vitro*. ***B***, Comparison of the HT bursting that occurs after Cch application (top left traces) with the tonic firing that is restored by Pzp (10 μM) (top right traces) in a different LGN TC neuron *in vitro*. The bottom left plot shows the relationship between HT burst frequency and steady current injection. The traces on the bottom right show a close comparison of the action potential output observed in Cch (red traces) and after Pzp application (blue traces). Note the presence of a prominent spike ADP when Cch is present, its clear involvement in HT burst generation, and its complete elimination after Pzp application.

HT bursting is a pervasive phenomenon in TC neurons of the LGN and VB after muscarinic receptor activation

Previous studies examining the effects of activating cholinergic receptors on cat TC neurons have not reported the presence HT bursting (McCormick and Prince, 1987; McCormick, 1992; Zhan et al., 2000). Thus, to fully assess the extent to which muscarinic receptor activation invokes HT bursting in the TC neuron population, we performed intracellular recordings from morphologically identified TC neurons in LGN and VB slices ($n = 50$). In control conditions, these cells exhibited a resting membrane potential (V_m) of −66.2 ± 2.4 mV ($n = 36$) and an apparent input resistance (R_N) of 190.4 ± 22.3 MΩ ($n = 36$) (Fig. 3*A*). In all cells, action potential output at depolarized membrane potentials in this condition was characterized solely by tonic firing (Fig. 4*A*). Consistent with previous studies (McCormick and Prince, 1987; McCormick, 1992), Cch application (50 μM) caused a rapid depolarization (19.1 ± 2.6 mV; $n = 20$) (Fig. 3*A*, top trace) that was initially associated with a pronounced reduction in R_N (15.3 ± 4.6% of control at 5 min; $n = 20$) (Fig. 3*A2*) but later by a significant increase in R_N (140.2 ± 10.1% of control at 20 min; $n = 20$) (Fig. 3*A3*). In the majority of TC neurons ($n = 37$ of 50; 74%), this depolarization led to either spontaneous tonic firing or to neurons expressing a V_m that was just below action potential threshold (Fig. 3*A*). Importantly, however, in both cases, action potential output at depolarized membrane potentials continued to consist exclusively of tonic firing (Fig. 3*A*). In marked contrast, in the remainder of TC neurons ($n = 13$ of 50; 26%), the Cch-induced depolarization led to spontaneous, rhythmic HT bursting at 8.6 ± 2.3 Hz ($n = 10$) (spikes per burst, 2.1 ± 0.05; ISI, 10.8 ± 0.7 ms; $n = 80$ bursts) (Figs. 3*B2*, 4*A*,*B*, 5*A*,*B*) (Hughes et al., 2002, 2004). Overall, HT bursting in TC neurons was of similar prevalence in the LGN ($n = 10$ of 36; 28%) (Figs. 3*B*, 4, 5*A*) and VB ($n = 3$ of 14; 21%) (Fig. 5*B*).

As is the case for mGluR1a-induced HT bursting (Hughes et al., 2004; Hughes and Crunelli, 2007), the interburst frequency for rhythmic HT bursting brought about by Cch application increased with increasing steady depolarizing current in the approximate range 3–15 Hz (Figs. 4*B*, bottom left, 5). In further correspondence with mGluR1a-induced bursting, a key cellular feature that facilitates the transformation of tonic firing into HT bursting during muscarinic activation was the appearance of a prominent spike afterdepolarization (ADP). Indeed, this ADP was clearly absent in control conditions (Fig. 4*A*) and was fully blocked after Pzp application ($n = 6$) (Fig. 4*B*, bottom right). As expected from extracellular recordings, all other effects of Cch observed with intracellular recordings could also be prevented ($n = 8$) (data not illustrated) or completely reversed ($n = 6$) (Fig. 3*B*) by Pzp (1–10 μM). The Cch-induced excitation of TC neurons was also antagonized by the M_3 receptor preferring blockers 4-DAMP (1–2 μM) (change in V_m, −9.5 ± 2.6 mV; $n = 6$) and DAU-5884 (1–2 μM) (change in V_m, −10.5 ± 2.6 mV; $n = 3$) (Fig. 3*C*) (supplemental Fig. 2*A*,*B*, available at www.jneurosci.org as supplemental material) but not by the M_1 receptor preferring antagonist Tzp (1 μM) (change in V_m, −1.4 ± 0.4 mV; $n = 6$)

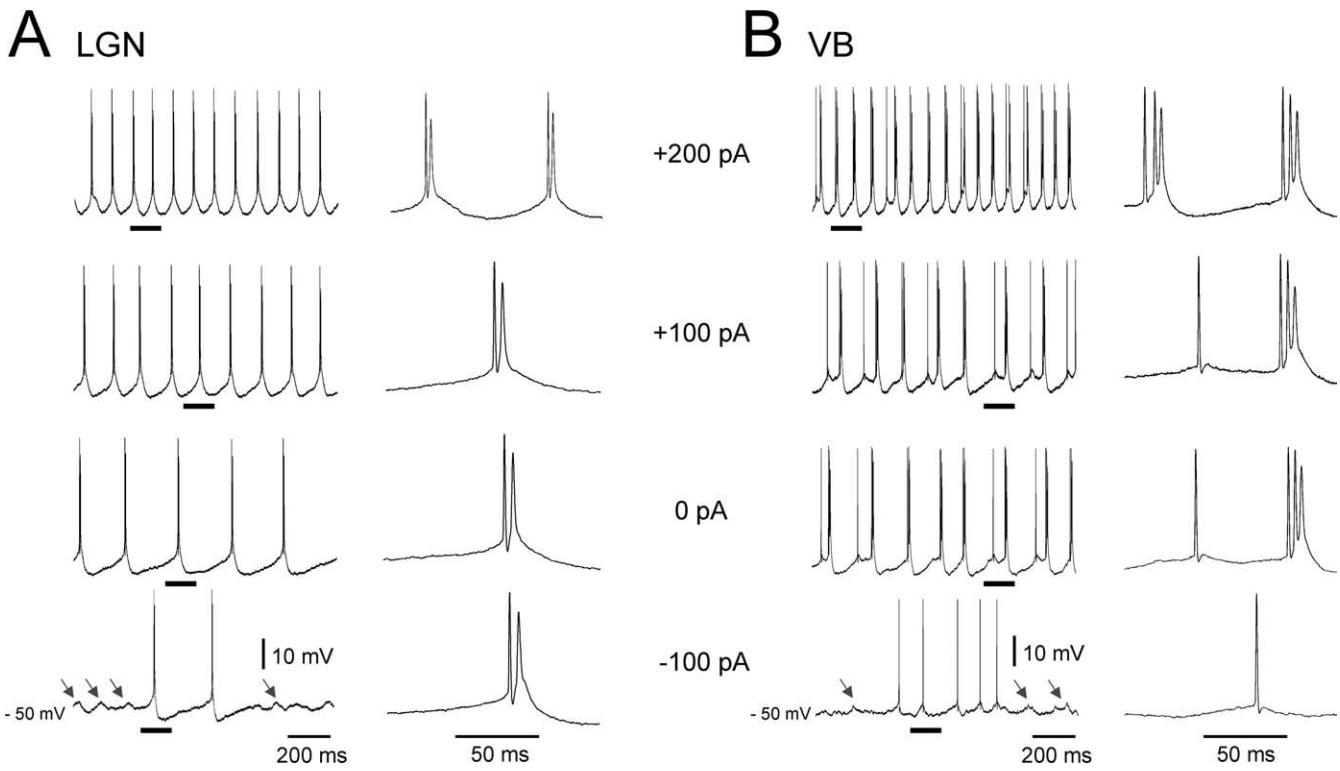

Figure 5. HT bursting TC neurons in the LGN and VB exhibit rhythmic, subthreshold depolarizing potentials during hyperpolarization. Intracellular recordings of HT bursting TC neurons from the LGN (***A***) and VB (***B***) at different levels of injected steady current as indicated. Note again the characteristic increase in frequency of rhythmic HT bursting as the cells are depolarized and the presence of subthreshold transient depolarizing events during steady hyperpolarization (arrows in bottom traces).

(Fig. 3*D*) (supplemental Fig. 2*A*, available at www.jneurosci.org as supplemental material).

Examination of the suprathreshold and subthreshold cellular dynamics of HT bursting TC neurons during cholinergically induced α rhythms

During isolated intracellular recordings of HT bursting TC neurons in the LGN and VB, we regularly observed rhythmic, subthreshold depolarizing potentials that we hypothesized to represent GJ-mediated network input from additional TC neurons (Fig. 5*A*,*B*, arrows) (Hughes et al., 2004; Hughes and Crunelli, 2005, 2007). To confirm this and so that we could better understand the cellular dynamics that control the output of HT bursting neurons during network oscillations, we performed intracellular recordings from HT bursting cells in the LGN while simultaneously monitoring the LFO with a proximal (<200 μm) extracellular electrode (Figs. 6–8) (see Fig. 10). All HT bursting LGN TC neurons were significantly correlated with ongoing network oscillations ($n = 13$; $p < 0.05$, Rao's spacing test) (Figs. 6–8) (see Fig. 10). As with extracellular recordings, in the absence of any steady injected current, these cells predominantly generated action potentials close to the negative LFO peak (6.7 ± 16.6°; $n = 8$) (Figs. 6–8) (see Fig. 10). Additionally, in the vast majority of cells ($n = 9$ of 13; 77%), a secondary cluster of spikes was also evident that occurred close to the positive LFO peak (167.8 ± 12.5°; $n = 7$) (Figs. 6, 7, red arrows in 8).

Hyperpolarization below action potential threshold in HT bursting cells commonly ($n = 6$ of 13; 46%) revealed unambiguous spikelets (i.e., action potentials generated in distinct cells that have been transmitted through an electrical synapse (Sohl et al., 2005) (duration, 8.6 ± 0.8 ms; amplitude, 1.5 ± 0.2 mV; $n = 40$ events) (Fig. 6*C*) (see Fig. 10*A*, blue arrows). Spikelets typically occurred in brief bursts (i.e., burstlets) (Hughes et al., 2004; Long et al., 2004) interspersed with single events (spikelets per burstlet, 2.2 ± 0.1; interspikelet interval, 14.1 ± 1.3 ms; $n = 20$ burstlets) (Fig. 6*C*) and were primarily evident near the negative LFO peak (14.5 ± 7.5°; $n = 4$ cells) (Fig. 6*D*) (see Fig. 10*B*) but sometimes switched to an antiphase relationship (195.0 ± 14.2°; $n = 4$) (Fig. 6*D*). Thus, spikelets entirely replicated action potential output from HT bursting neurons, confirming that these cells are interconnected by GJs. Importantly, within all cells in which unambiguous spikelets were present, their properties were very well conserved (Fig. 6*C*,*D*), indicating that the dominant network input to these cells arises from one, or very few, additional cells. In some HT bursting neurons ($n = 5$ of 13; 38%), although the presence of rhythmic subthreshold network-related activity was clearly present (Figs. 7*B*, 8*B*), we did not observe unequivocal individual spikelets or burstlets. However, the average subthreshold activity of these cells, triggered by the negative peak of the LFO, often revealed clear and correlated rhythmic burstlets, indicating that these cells are also the recipients of discrete, oscillation-related GJ-mediated input from additional HT bursting cells (Fig. 7*B*, bottom right).

Phase preference in HT bursting TC neurons is modulated by membrane polarization

In some HT bursting cells that exhibited extensive phase-shifting in their spiking output, despite the fact that clear antiphase subthreshold network input was present, the dominant and overwhelming network input still occurred in-phase with the negative LFO peak ($n = 3$) (Fig. 7). Consistent with previous work (Hughes et al., 2004; Hughes and Crunelli, 2007), this suggested that extensive phase shifting most likely results from a complex interaction between network input and the intrinsic bursting

properties of individual cells. To investigate this further, we examined the effect of injecting different quantities of steady current on the phase preference of action potential output in HT bursting TC neurons (Fig. 8*A*). In all cells in which we performed this experiment ($n = 7$), we observed a stereotyped sequence of events whereby, during gradual depolarization from below threshold (Fig. 8*B*), action potential output first predominantly occurred close to the negative LFO peak and then gradually shifted toward an earlier phase before being transformed into an overt phase-shifting pattern (Fig. 8*A*,*C*). Thus, the phase of the LFO at which HT bursting cells preferentially fire and the presence of phase-shifting can be dynamically modulated and are determined by a combination of network input, intrinsic properties, and membrane polarization.

A small proportion of tonic firing TC neurons are also engaged in local α activity by GJs

Interestingly, hyperpolarization of some tonic firing TC neurons ($n = 4$ of 18; 22%) below action potential threshold also revealed rhythmic spikelets and burstlets (see Figs. 9*A*,*B*, 10*C*) that primarily occurred near the negative LFO peak (16.8 ± 10.4°; $n = 4$) but that sometimes shifted to an antiphase pattern (165.8 ± 13.7°; $n = 4$) (see Fig. 9*B*, 10*C*). Spikelets in tonic firing cells often occurred in brief bursts and had temporal properties that were indistinguishable from those observed in HT bursting cells (duration, 8.5 ± 0.5 ms; spikelets per burstlet, 2.3 ± 0.1; interspikelet interval, 10.7 ± 0.8 ms; $n = 20$ events and $p > 0.25$ for each case), suggesting that these cells are directly connected to HT bursting cells via GJs (Hughes et al., 2004, their Fig. 7*B*). Although the mean amplitude of spikelets was significantly smaller than in HT bursting cells (0.8 ± 0.1 mV; $p < 0.001$; $n = 20$ events), action potential timing could be closely aligned to, and remarkably well predicted by, this presumed GJ-mediated network input so that action potentials in these cells also occurred predominantly close to the negative peak of the LFO (Fig. 9*B*). In agreement with this, simultaneous extracellular recordings of HT bursting and tonic firing TC neurons often exhibited a moderate degree of synchronous firing (Fig. 9*C*) (see also Fig. 3*C*, right traces).

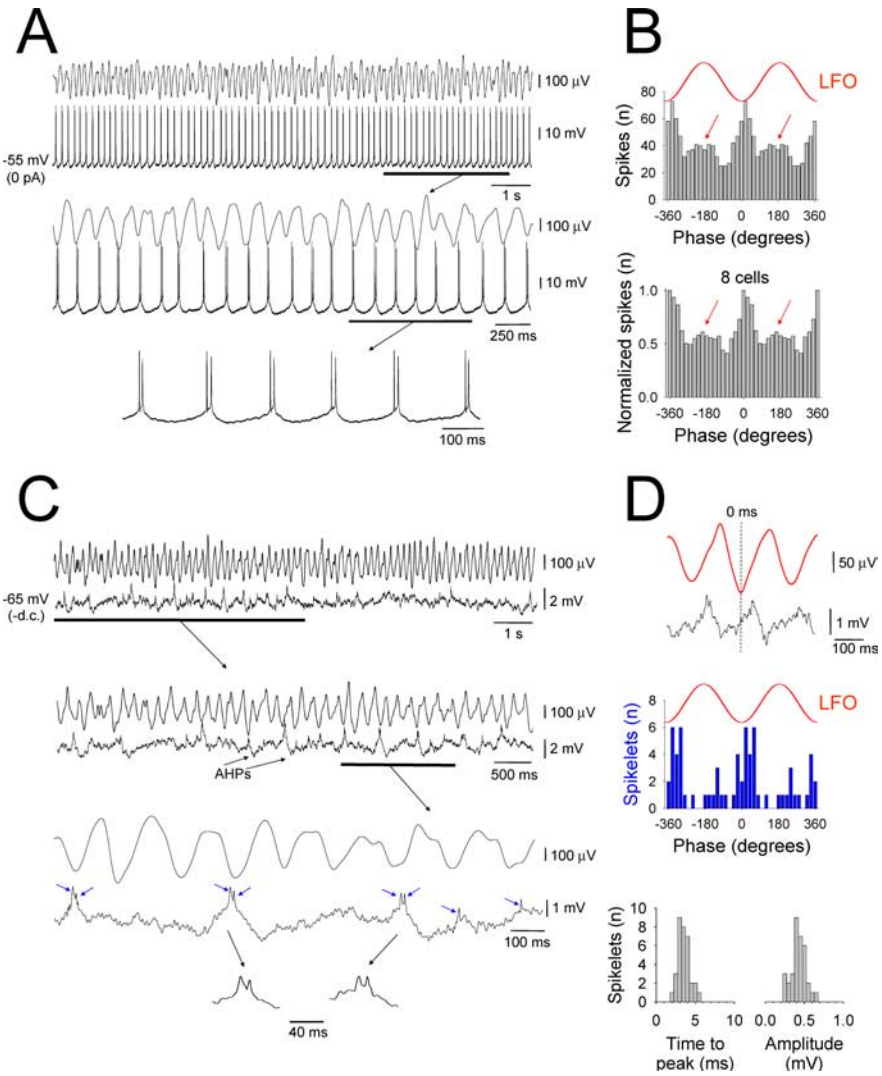

Figure 6. Suprathreshold and subthreshold membrane potential dynamics of an individual HT bursting TC neuron in the LGN during network α activity. ***A***, Simultaneous field recording of the Cch-induced (50 μM) α LFO and intracellular recording of an HT bursting TC neuron in the cat LGN *in vitro*. The underlined section is expanded below and reveals a clear correlation between the LFO and TC neuron firing. The additional expansion below illustrates the robust, rhythmic nature of the HT bursting activity. ***B***, The correlation between the LFO and TC neuron shown in ***A*** is clearly evident in the corresponding spike timing histogram (top). Note the small cluster of spikes that occur in an antiphase relationship to the negative LFO peak (red arrows). The plot below represents the pooled output of eight different HT bursting cells recorded intracellularly in the LGN. Again, note the presence of both in-phase and antiphase peaks. ***C***, Activity of the TC neuron in ***A*** after hyperpolarization below action potential threshold. The underlined section is expanded below and shows the presence of depolarizing events that are followed by an afterhyperpolarization (AHP) and that appear to occur predominantly close to the negative LFO peak. The further expansion reveals that these events comprise an underlying slow depolarization that is crowned by spikelets (pairs of blue arrows), i.e., a burstlet. These burstlets are also intermingled with single spikelet events (indicated by single blue arrows). ***D***, Top two traces, Average of the intracellular membrane potential (black trace) triggered by the negative peak of the LFO for the epoch shown in ***C***. The red trace is the corresponding average LFO. Middle section, Spikelet timing histogram confirming that the majority of these events occur close to the negative field peak but that a small cluster also occur antiphasically. Bottom section, Distribution of time-to-peak (bin size, 0.5 ms) and amplitude (bin size, 0.05 mV) of spikelets from the cell in ***C***. In both cases, the narrow distribution reflects a conserved all-or-none appearance.

Single HT bursting TC neurons can potently influence the local network state

Given that both HT bursting cells and some tonic firing cells are engaged in network oscillations by GJs, we asked to what extent their different forms of output can influence the overall oscillatory state of the local network. To address this, we examined the effect of a brief period of continuous HT bursting or tonic firing in an individual neuron on the amplitude of the local α field oscillation. Specifically, we held single TC neurons below firing threshold with steady hyperpolarizing current for an extended period after impalement (≥2 min) and then compared the mean peak-to-peak amplitude of the LFO in this condition with that observed in the 20 s immediately subsequent to a period of at least 20 s when the neurons were allowed to fire continuously (Fig.

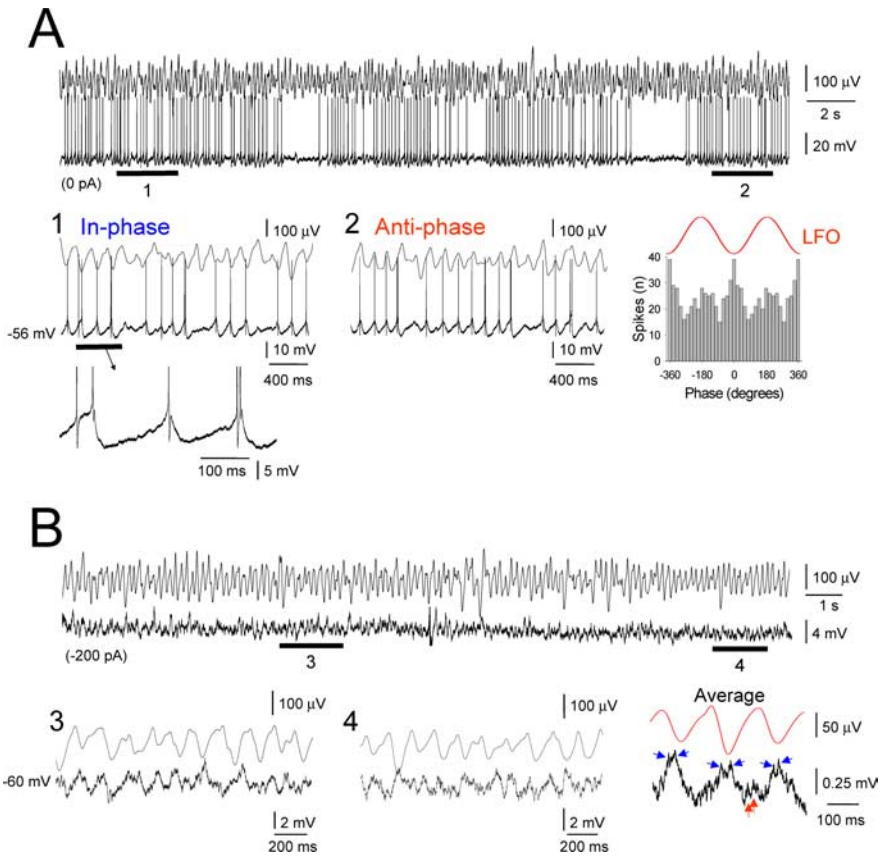

Figure 7. Extensive phase-shifting in an HT bursting TC neuron in the LGN assessed with intracellular recording. ***A***, Example of extensive and overt phase-shifting observed intracellularly in an LGN TC neuron *in vitro*. The underlined sections from the top trace are enlarged below and show HT bursting dynamically shifting between periods of in-phase (***1***) and antiphase (***2***) activity (compare Fig. 2*B*). The corresponding spike timing histogram is shown to the right. Note that, in this neuron, bursting does not occur continuously which is consistent with the demonstration in Figure 6*C* that GJ-mediated input does not necessarily occur on every oscillation cycle. ***B***, Subthreshold activity of the neuron shown in ***A*** obtained after hyperpolarization. The underlined sections (***3***, ***4***) are expanded below, and, although individual burstlet events are not obviously present, the corresponding LFO negative peak-triggered subthreshold membrane potential average to the right clearly reveals that this cell is subject to discrete GJ-mediated input from an additional HT bursting cell (blue and red arrows indicate in-phase and antiphase spikelets, respectively. Note that the very small antiphase subthreshold input is unlikely to alone explain the large amount of antiphase action potential output observed in this neuron during depolarization as shown in ***A***.

10*A*). In doing so, we found that the mean peak-to-peak field amplitude was significantly greater in the 20 s after HT bursting than in the initial hyperpolarized period (118.4.9 ± 5.1% of control; $n = 8$ trials from 8 cells; $p < 0.01$) (Fig. 10*A*,*B*). Furthermore, in some cases, when neurons were again subjected to the same level of hyperpolarizing current that was present during the initial phase, some of them continued to exhibit action potential output that was correlated to the LFO rather than become quiescent ($n = 2$ of 8; 25%) (Fig. 10*A4*). In contrast, a brief period of tonic firing did not appreciably influence the LFO (peak-to-peak amplitude in the 20 s after the firing epoch, 97.8 ± 2.1% of control; $n = 12$ trials from 4 cells; $p > 0.5$) (Fig. 10*C*,*D*). Thus, a single HT bursting TC neuron is able to potently influence the local network, whereas an individual tonic firing cell is not.

Discussion

This study greatly extends the previously known consequences of cholinergic activation on the thalamus. The specific main findings are as follows. (1) Activation of muscarinic ACh receptors in slices of the cat LGN and VB elicits synchronized oscillations at α frequencies. (2) These oscillations are shaped by a GJ-coupled subnetwork of HT bursting TC neurons. (3) The appearance of HT bursting after muscarinic receptor activation is fundamentally reliant on the instatement of a prominent spike ADP. (4) HT bursting can exhibit a complex dynamic relationship with ongoing network oscillations, often spontaneously switching between an in-phase and antiphase association with the negative LFO peak. More generally, the phase of the LFO at which HT bursting cells prefer to generate action potentials and the appearance of phase shifting are determined by the combined effects of network input, intrinsic properties, and membrane polarization. (5) Single HT bursting TC neurons are able to powerfully influence the local network state, whereas individual tonic firing cells are not. In concert with previous work (Hughes et al., 2004; Hughes and Crunelli, 2005), these results show that sensory thalamic nuclei contain powerful and dynamically reconfigurable mechanisms for generating robust α rhythms that can be enlisted by both descending and ascending arousal systems.

Relationship to previous *in vitro* studies

An important and fundamental new finding of this study is that muscarinic receptor activation can induce intrinsic HT bursting in a subset of TC neurons of the LGN and VB. Thus, the excitatory effect of activating muscarinic receptors on TC neurons is not always to simplistically switch the firing mode from LTCP-mediated bursting toward tonic action potential output but can be to fundamentally change the properties of cells so that they become more facilitating of network oscillations, as shown for other neuronal types (Lawrence et al., 2006b; Tai et al., 2006). In this sense, TC neurons appear to behave more like neocortical neurons, which are flexible entities that readily change their firing mode depending on the local neuromodulatory conditions (Steriade, 2004). The instigation of HT bursting by Cch is also striking because several previous *in vitro* studies investigating the effects of activating cholinergic receptors on TC neurons have failed to observe this phenomenon (McCormick and Prince, 1987; McCormick, 1992; Zhu and Uhlrich, 1998; Zhan et al., 2000). In some of these studies, experiments were performed on the rat (Zhu and Uhlrich, 1998) or guinea pig (McCormick and Prince, 1987; McCormick, 1992) thalamus or on the cat auditory thalamus, i.e., the medial geniculate body (McCormick and Prince, 1987), suggesting that HT bursting might be restricted to the somatosensory and visual thalamus of higher mammals, an idea that is partly in keeping with a recent study looking at nucleus- and species-related differences in the effects of mGluR activation on TC neurons (Zhu et al., 2006). However, as to why HT bursting was not observed in previous *in vitro* experiments performed in the cat LGN may be attributable to numerous factors, including the use of ACh or acetyl-β-methylcholine to activate cholinergic receptors rather than Cch (McCormick and Prince, 1987), a lower concentration of Cch (Zhan et al., 2000), or

a lower initial R_N. Nevertheless, the majority of TC neurons in this study still generated tonic action potentials after muscarinic activation. Furthermore, a small proportion of these are entrained in network oscillations via GJ connections with HT bursting cells, suggesting that, although single HT bursting neurons can potently influence the local network (see below), the overall population oscillation may be an emergent property of a both cell types. This raises the important of question of what occurs to the remaining majority of tonic cells during α rhythms. With respect to this, our preliminary data suggests that these cells are not entrained in α activity in any consistent manner but do receive phasic inhibition from local circuit interneurons, which themselves are directly excited by HT bursting cells (our unpublished observations).

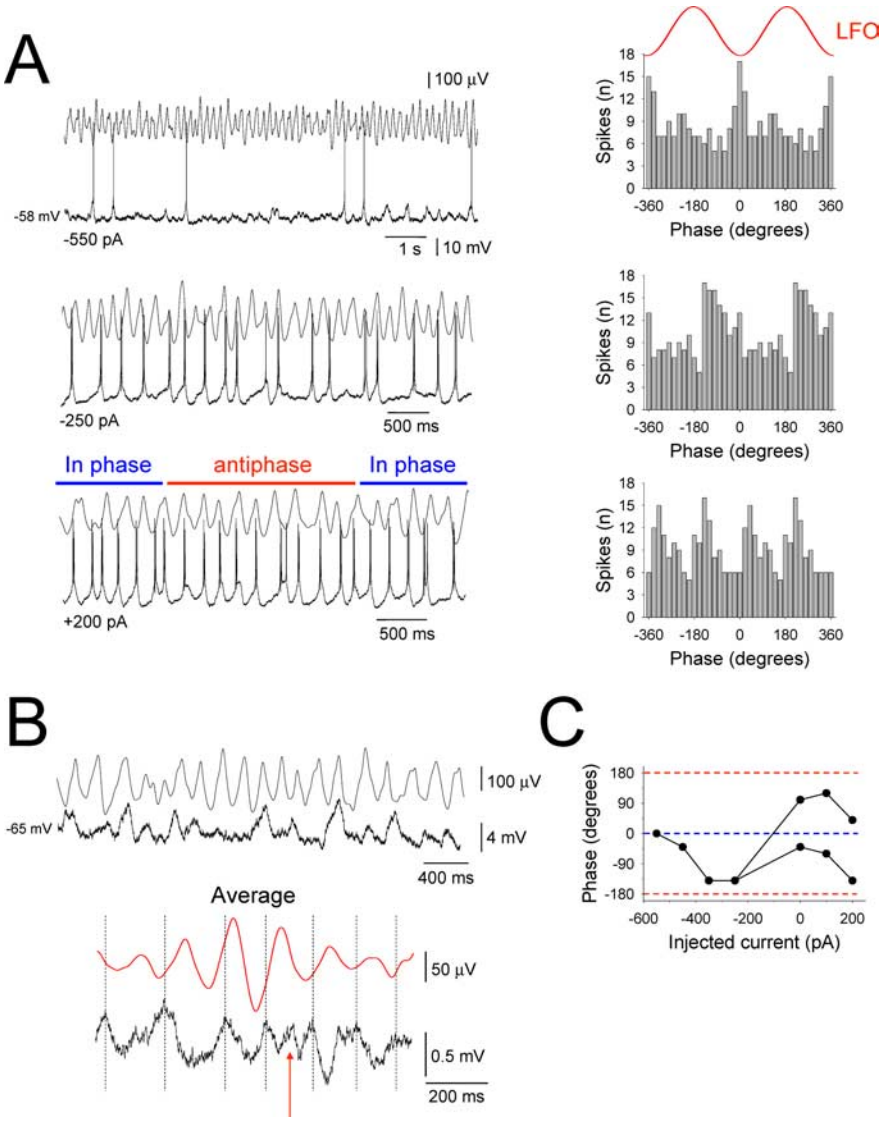

Figure 8. LFO-related spike output patterns in HT bursting TC neurons are determined by a combination of network input, intrinsic properties, and membrane polarization. ***A***, Activity of an HT bursting TC neuron in the LGN *in vitro* during ongoing network α oscillations at different levels of steady injected current as indicated. The corresponding spike timing histograms are shown on the right and reveal that, as the cell is progressively depolarized, spike phase preference changes from a predominantly in-phase pattern (top) to a more overt phase-shifting pattern (bottom). ***B***, Activity of the same neuron after hyperpolarization below action potential threshold illustrating that subthreshold network input appears to occur predominantly close to the negative LFO peak. This is verified by the LFO negative peak-triggered subthreshold membrane potential average shown below, although a clear anti-phase input is also revealed (red arrow). ***C***, Plot providing a more comprehensive representation of the phase preference of the neuron depicted in this figure for different amounts of steady current. Different points in the plot represent distinct peaks in the spike timing histograms (see ***A***).

Comparison of mGluR1a- and muscarinic receptor-mediated effects on thalamic network activity

Activating mGluR1a also brings about α oscillations in the LGN that are shaped by HT bursting and GJs (Hughes et al., 2004; Hughes and Crunelli, 2005). However, unlike the oscillations described here, mGluR1a-induced rhythms are of smaller amplitude (typically 40–50 vs ~150 μV peak-to-peak amplitude). This suggests that, although they are very similar, there are some key differences in the mechanisms that lead to α oscillations in the two cases. This is not entirely surprising because, although the postsynaptic targets of mGluR1a and muscarinic receptors are certainly alike, they are unlikely to be identical. In addition, the location of these receptors on the somatodendritic axis of TC neurons is also distinct with mGluR1a being situated at more distal sites (Erisir et al., 1997a,b). Another possibility is that mGluR1a and muscarinic receptors differentially influence GJ function in TC neurons. For example, it is now known that mGluR activation in neurons of the thalamic reticular nucleus can lead to a persistent reduction in coupling strength (Landisman and Connors, 2005), a phenomena that may also occur in TC neurons. That mGluR1a and muscarinic receptor activation can recruit different mechanisms to promote network oscillations at similar frequencies has also been demonstrated in the hippocampal CA3 region (Palhalmi et al., 2004) and clearly points to the fact that, in various brain areas, mGluR1a and muscarinic receptors have related, but distinct, roles in controlling network oscillations.

Mechanisms and potential functional significance of phase shifting

A common feature of both mGluR1a and muscarinic receptor-induced α oscillations is that HT bursting neurons can exhibit a dynamic phase relationship with the ongoing field oscillation, often spontaneously switching between an in-phase and antiphase association (Hughes et al., 2004; Hughes and Crunelli, 2007). This dynamic phase intonation contrasts markedly with that which occurs in other brain areas, such as the hippocampus, in which the firing patterns of neurons of a similar type are remarkably stereotypical and exhibit a reproducible monophasic relationship with respect to the ongoing field oscillations (Klausberger et al., 2003, 2004; Hajos et al., 2004). Interestingly, dynamic phase shifting in the thalamus dictates that, at any point in time, the local network state essentially reflects the destructive interference between two populations of neurons that oscillate in an essentially antiphase relationship to each other (Hughes et al.,

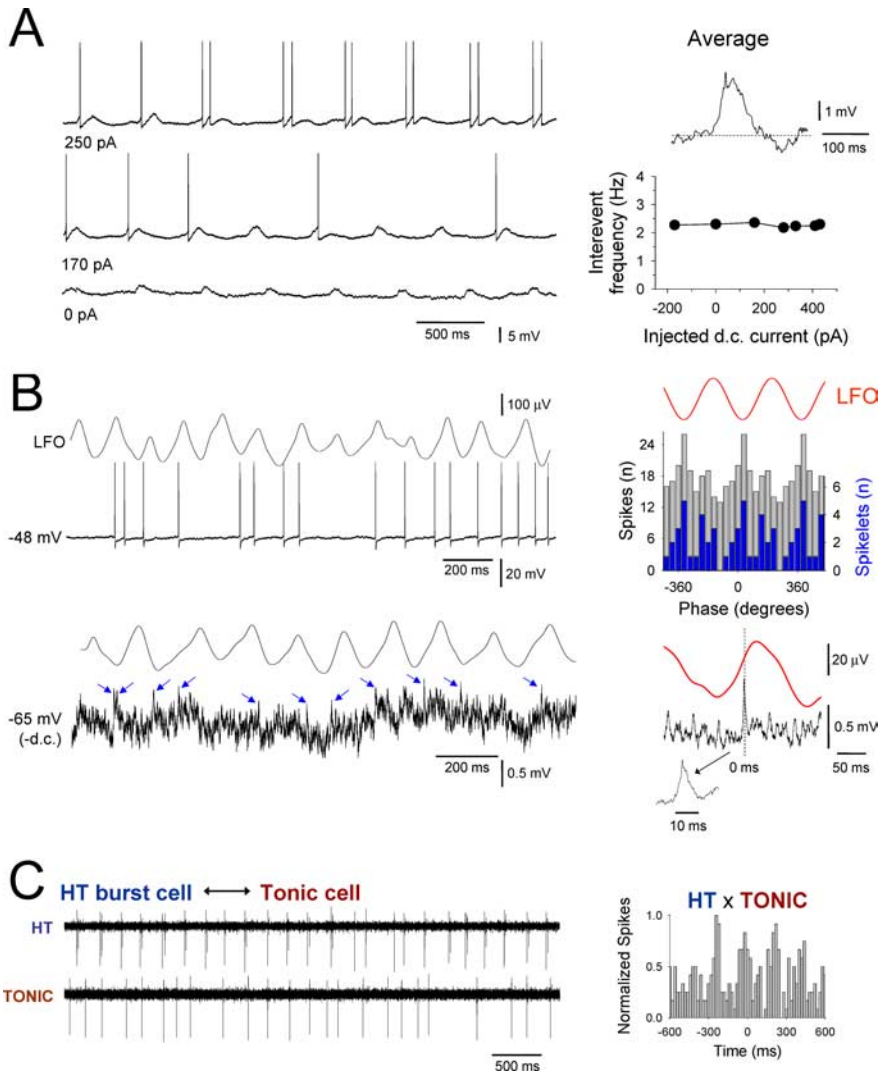

Figure 9. A small subset of tonic firing TC neurons are also entrained into network α activity via GJ connections with HT burst cells. ***A***, Intracellular recording of a tonic firing LGN TC neuron in the presence of 50 μM Cch showing entrainment of firing by rhythmic potentials. An average of these potentials reveals a clear burstlet waveform (top right trace) indicating that some tonic firing cells receive direct GJ-mediated input from HT bursting neurons. The invariance of the frequency of these events with respect to membrane polarization also clearly indicates a network, rather than intrinsic, origin (bottom right plot). ***B***, Simultaneous recording of the LFO and intracellular activity of a tonic firing TC neuron. Shown below is the activity of this neuron after hyperpolarization. The blue arrows indicate putative spikelets. The corresponding spike (gray bars) and spikelet (blue bars) timing histograms are shown to the top right. The spikelet-triggered LFO average is shown at the bottom right. ***C***, HT bursting cell (top) and tonic firing cell (bottom) recorded in the presence of 50 μM Cch with independent extracellular electrodes. The corresponding cross-correlogram is shown on the right and reveals a moderate degree of synchrony between the two cells.

2004, 2007). Because phase shifting appears to be a response to increasing depolarization, one prediction of this scheme is that the reduction of gross α waves that occurs in the intact brain with increased attention, and particularly on eye opening, may not necessarily reflect a decrease in cellular α activity (Hughes et al., 2004).

We recently hypothesized that one of the reasons that HT bursting TC neurons can exhibit a dynamic phase shifting pattern is because, like GJ-coupled networks of excitatory neurons in other brain areas (Draguhn et al., 1998; Traub and Bibbig, 2000), they are sparsely connected (Hughes et al., 2004; Hughes and Crunelli, 2007). The current study strongly endorses this view because (1) the subthreshold network-derived input to single cells is often manifested as unambiguous spikelets that within that cell display a conserved all-or-none appearance, indicating a probable origin from one or very few other neurons (Fig. 6*C*), and (2) even when unambiguous individual spikelets are not apparent, the LFO-triggered subthreshold average reveals discrete GJ-mediated input (Fig. 7*B*). One upshot of this sparse coupling appears to be that single HT bursting cells are able to exert a greater degree of influence on surrounding cells, probably via a domino effect, ultimately enabling them to discernibly alter the proximal LFO.

Cholinergic input, network oscillations, and brain functioning

Although the classical view of α rhythms is that they reflect an idling state of primary cortical areas, there is a long history of research indicating that they also play important roles in a variety of cognitive processes, aspects of sensory perception, and memory operations (Bartley, 1940; Lindsley, 1952; Varela et al., 1981; VanRullen and Koch, 2003). For example, both reaction time (Surwillo, 1961) and the maximal interstimulus interval for simultaneity judgment (Kristofferson, 1967) are highly correlated with α rhythm frequency. In addition, several studies have shown close links between α band oscillations and different types of long-term memory processes (Klimesch, 1999). Given the known involvement of the cholinergic system in bringing about oscillations in other brain areas that are intimately linked to cognitive function and memory processing (Huerta and Lisman, 1993; Fisahn et al., 1998, 2002; Mann et al., 2005; Traub et al., 2005; Oren et al., 2006), we suggest that the finding that activating muscarinic receptors induces robust and dynamically complex α oscillations in sensory thalamic nuclei is consistent with the concept that EEG α rhythms in the whole organism represent far more than a simple standby condition. Finally, given the importance of the cholinergic system in generating normal α activity indicated by this study, it is tempting to speculate that a shortfall in thalamic ACh may explain the α rhythm slowing that occurs in cognitive disorders such as Alzheimer's disease and schizophrenia (Soininen et al., 1992; Hughes and Crunelli, 2005).

References

Adrian ED, Matthews (1934) The Berger rhythm: potential changes from the occipital lobes in man. Brain 57:355–385.

Adrian ED, Yamagiwa K (1935) The origin of the Berger rhythm. Brain 58:323–351.

Bartley SH (1940) The relationship between cortical responses to visual stimulation and changes in the alpha rhythm. J Exp Psychol 27:624–639.

Berger H (1929) Über das elektroenkaphogramm des menschen. Archiv für Psychiatrie und Nervenkrankheiten 87.

Blethyn KL, Hughes SW, Toth TI, Cope DW, Crunelli V (2006) Neuronal basis of the slow (<1 Hz) oscillation in neurons of the nucleus reticularis thalami *in vitro*. J Neurosci 26:2474–2486.

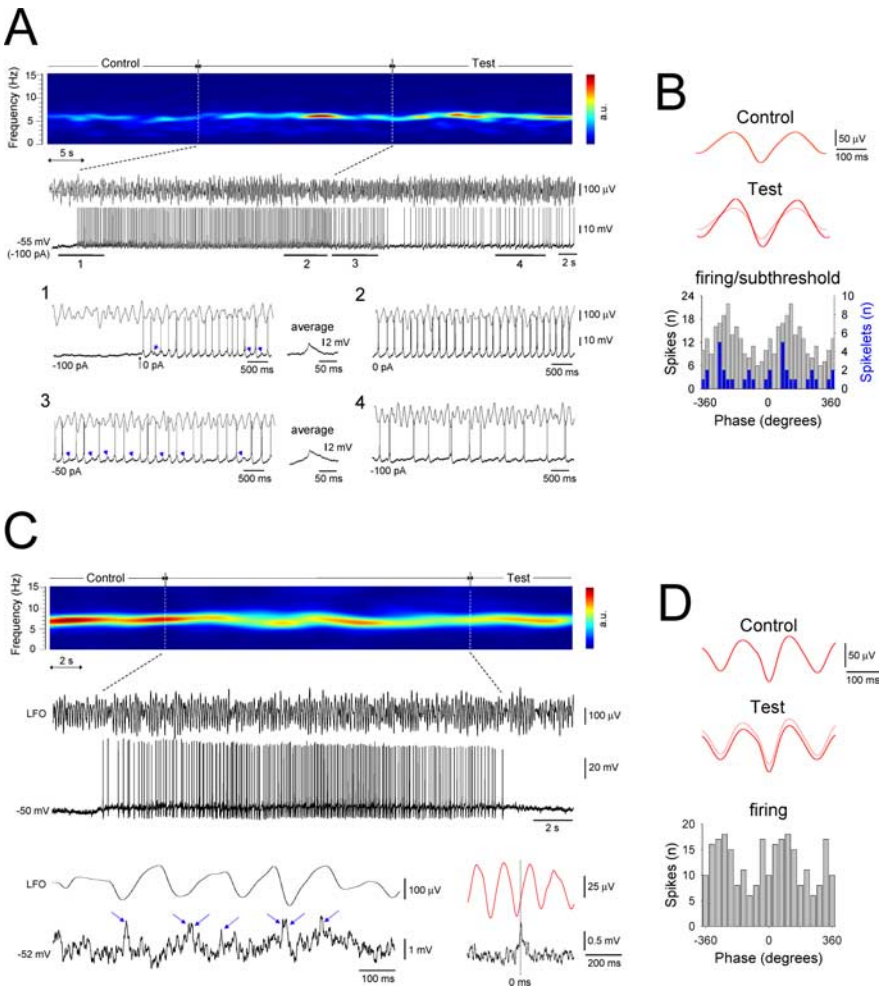

Figure 10. A single HT bursting TC neuron can potently influence local network activity, whereas an individual tonic firing cannot. ***A***, Spectrogram of a 70 s segment of Cch-induced α activity *in vitro*. The raw LFO and a simultaneous recording of an HT bursting TC neuron in the LGN are shown below. The neuron is initially held below threshold with steady current but is later allowed to burst spontaneously for ~30 s. In ***1***, the neuron is released from hyperpolarization and exhibits HT bursting. GJ-mediated input also becomes evident (blue arrows, averaged and enlarged to the right), indicating the activation of an additional neuron. In ***2***, the neuron bursts continuously in close correlation with the LFO. In ***3***, slight hyperpolarization (−50 pA) again reveals GJ-mediated input. In ***4***, steady current is returned to −100 pA (as in the initial subthreshold phase), but the neuron continues to show some field-correlated firing. ***B***, Top, LFO average for the initial subthreshold control period in ***A*** (triggered by the negative LFO peak). Bottom, LFO average for the 20 s test period immediately after the induced bursting (red trace). The light red trace is a superimposition of the average LFO in the control period. Corresponding spike (gray bars) and spikelet (blue bars) timing histograms, constructed from sections ***1–3*** in ***A***, are shown below. ***C***, Spectrogram of a 32 s period of Cch-induced α activity. The raw LFO and a simultaneous recording of a tonic firing TC neuron are shown below. Shown further below is a brief section of the subthreshold membrane potential from this cell, which clearly shows the presence of spikelets and burstlets (individual spikelets are indicated by the blue arrows) (left) and the spikelet-triggered LFO average (right). ***D***, Top, Average LFO for the initial subthreshold control period in ***C*** (triggered by the negative LFO peak). Bottom, LFO average for the 20 s test period immediately after the induced firing (red trace). The light red trace is a superimposition of the average LFO in the control period. The corresponding spike timing histogram is shown below.

Bouyer JJ, Rougeul A, Buser P (1982) Somatosensory rhythms in the awake cat: a single unit exploration of their thalamic concomitant in nucleus ventralis posterior and vicinity. Arch Ital Biol 120:95–110.

Bouyer JJ, Tilquin C, Rougeul A (1983) Thalamic rhythms in cat during quiet wakefulness and immobility. Electroencephalogr Clin Neurophysiol 55:180–187.

Chatila M, Milleret C, Buser P, Rougeul A (1992) A 10 Hz "alpha-like" rhythm in the visual cortex of the waking cat. Electroencephalogr Clin Neurophysiol 83:217–222.

Chatila M, Milleret C, Rougeul A, Buser P (1993) Alpha rhythm in the cat thalamus. C R Acad Sci III 316:51–58.

Davidson JS, Baumgarten IM (1988) Glycyrrhetinic acid derivatives: a novel class of inhibitors of gap-junctional intercellular communication. Structure-activity relationships. J Pharmacol Exp Ther 246:1104–1107.

de Lima AD, Montero VM, Singer W (1985) The cholinergic innervation of the visual thalamus: an EM immunocytochemical study. Exp Brain Res 59:206–212.

Draguhn A, Traub RD, Schmitz D, Jefferys JG (1998) Electrical coupling underlies high-frequency oscillations in the hippocampus in vitro. Nature 394:189–192.

Erisir A, Van Horn SC, Sherman SM (1997a) Relative numbers of cortical and brainstem inputs to the lateral geniculate nucleus. Proc Natl Acad Sci USA 94:1517–1520.

Erisir A, Van Horn SC, Bickford ME, Sherman SM (1997b) Immunocytochemistry and distribution of parabrachial terminals in the lateral geniculate nucleus of the cat: a comparison with corticogeniculate terminals. J Comp Neurol 377:535–549.

Fisahn A, Pike FG, Buhl EH, Paulsen O (1998) Cholinergic induction of network oscillations at 40 Hz in the hippocampus in vitro. Nature 394:186–189.

Fisahn A, Yamada M, Duttaroy A, Gan J-W, Deng CX, McBain CJ, Wess J (2002) Muscarinic induction of hippocampal gamma oscillations requires coupling of the M1 receptor to two mixed cation currents. Neuron 33:615–624.

Godwin DW, Vaughan JW, Sherman SM (1996a) Metabotropic glutamate receptors switch visual response mode of lateral geniculate nucleus cells from burst to tonic. J Neurophysiol 76:1800–1816.

Godwin DW, Van Horn SC, Eriir A, Sesma M, Romano C, Sherman SM (1996b) Ultrastructural localization suggests that retinal and cortical inputs access different metabotropic glutamate receptors in the lateral geniculate nucleus. J Neurosci 16:8181–8192.

Hajos N, Palhalmi J, Mann EO, Nemeth B, Paulsen O, Freund TF (2004) Spike timing of distinct types of GABAergic interneuron during hippocampal gamma oscillations *in vitro*. J Neurosci 24:9127–9137.

Huerta PT, Lisman JE (1993) Heightened synaptic plasticity of hippocampal CA1 neurons during a cholinergically induced rhythmic state. Nature 364:723–725.

Hughes SW, Crunelli V (2005) Thalamic mechanisms of EEG alpha rhythms and their pathological implications. The Neuroscientist 11:357–372.

Hughes SW, Crunelli V (2007) Just a phase they're going through: the complex interaction of intrinsic high-threshold bursting and gap junctions in the generation of thalamic alpha and theta rhythms. Int J Psychophysiol 64:3–7.

Hughes SW, Cope DW, Blethyn KL, Crunelli V (2002) Cellular mechanisms of the slow (<1 Hz) oscillation in thalamocortical neurons in vitro. Neuron 33:947–958.

Hughes SW, Lorincz M, Cope DW, Blethyn KL, Kekesi KA, Parri HR, Juhasz G, Crunelli V (2004) Synchronized oscillations at alpha and theta frequencies in the lateral geniculate nucleus. Neuron 42:253–268.

Klausberger T, Magill PJ, Marton LF, Roberts JD, Cobden PM, Buzsaki G, P. S (2003) Brain-state- and cell-type-specific firing of hippocampal interneurons in vivo. Nature 421:844–848.

Klausberger T, Marton LF, Baude A, Roberts JD, Magill PJ, Somogyi P (2004)

Spike timing of dendrite-targeting bistratified cells during hippocampal network oscillations in vivo. Nat Neurosci 7:41–47.
Klimesch W (1999) EEG alpha and theta oscillations reflect cognitive and memory performance: a review and analysis. Brain Res Brain Res Rev 29:169–195.
Kristofferson AB (1967) Successiveness discrimination as a two-state, quantal process. Science 158:1337–1339.
Landisman CE, Connors BW (2005) Long-term modulation of electrical synapses in the mammalian thalamus. Science 310:1809–1813.
Lawrence JJ, Statland JM, Grinspan ZM, McBain CJ (2006a) Cell-type specific dependence of muscarinic signalling in mouse hippocampal stratum oriens interneurones. J Physiol (Lond) 570:595–610.
Lawrence JJ, Grinspan ZM, Statland JM, McBain CJ (2006b) Muscarinic receptor activation tunes mouse stratum oriens interneurones to amplify spike reliability. J Physiol (Lond) 571:555–562.
Leresche N, Lightowler S, Soltesz I, Jassik-Gerschenfeld D, Crunelli V (1991) Low-frequency oscillatory activities intrinsic to rat and cat thalamocortical cells. J Physiol (Lond) 441:155–174.
Lindsley DB (1952) Psychological phenomena and the electroencephalogram. Electroencephalogr Clin Neurophysiol 4:443–456.
Long MA, Landisman CE, Connors BW (2004) Small clusters of electrically coupled neurons generate synchronous rhythms in the thalamic reticular nucleus. J Neurosci 24:341–349.
Lopes da Silva FH, van Lierop TH, Schrijer CF, van Leeuwen WS (1973a) Organization of thalamic and cortical alpha rhythms: spectra and coherences. Electroencephalogr Clin Neurophysiol 35:627–639.
Lopes da Silva FH, van Lierop TH, Schrijer CF, van Leeuwen WS (1973b) Essential differences between alpha rhythms and barbiturate spindles: spectra and thalamo-cortical coherences. Electroencephalogr Clin Neurophysiol 35:641–645.
Mann EO, Suckling JM, Hajos N, Greenfield SA, Paulsen O (2005) Perisomatic feedback inhibition underlies cholinergically induced fast network oscillations in the rat hippocampus in vitro. Neuron 45:105–117.
McCormick DA (1992) Cellular mechanisms underlying cholinergic and noradrenergic modulation of neuronal firing mode in the cat and guinea pig dorsal lateral geniculate nucleus. J Neurosci 12:278–289.
McCormick DA, Prince DA (1987) Actions of acetylcholine in the guinea-pig and cat medial and lateral geniculate nuclei, in vitro. J Physiol (Lond) 392:147–165.
McCormick DA, von Krosigk M (1992) Corticothalamic activation modulates thalamic firing through glutamate "metabotropic" receptors. Proc Natl Acad Sci USA 89:2774–2778.
Oren I, Mann EO, Paulsen O, Hajos N (2006) Synaptic currents in anatomically identified CA3 neurons during hippocampal gamma oscillations *in vitro*. J Neurosci 26:9923–9934.
Palhalmi J, Paulsen O, Freund TF, Hajos N (2004) Distinct properties of carbachol- and DHPG-induced network oscillations in hippocampal slices. Neuropharmacology 47:381–389.
Pfurtscheller G, Neuper C, Andrew C, Edlinger G (1997) Foot and hand area mu rhythms. Int J Psychophysiol 26:121–135.
Pineda JA (2005) The functional significance of mu rhythms: translating "seeing" and "hearing" into "doing". Brain Res Brain Res Rev 50:57–68.
Pirchio M, Turner JP, Williams SR, Asprodini E, Crunelli V (1997) Postnatal development of membrane properties and delta oscillations in thalamocortical neurons of the cat dorsal lateral geniculate nucleus. J Neurosci 17:5428–5444.
Plummer KL, Manning KA, Levey AI, Rees HD, Uhlrich DJ (1999) Muscarinic receptor subtypes in the lateral geniculate nucleus: a light and electron microscopic analysis. J Comp Neurol 404:408–425.
Rougeul-Buser A, Buser P (1997) Rhythms in the alpha band in cats and their behavioural correlates. Int J Psychophysiol 26:191–203.
Rougeul-Buser A, Bouyer JJ, Buser P (1975) From attentiveness to sleep. A topographical analysis of localized "synchronized" activities on the cortex of normal cat and monkey. Acta Neurobiol Exp (Warsz) 35:805–819.
Sohl G, Maxeiner S, Willecke K (2005) Expression and functions of neuronal gap junctions. Nat Rev Neurosci 6:191–200.
Soininen H, Reinikainen KJ, Partanen J, Helkala EL, Paljarvi L, Riekkinen PJ (1992) Slowing of electroencephalogram and choline acetyltransferase activity in post mortem frontal cortex in definite Alzheimer's disease. Neuroscience 49:529–535.
Steriade M (2004) Neocortical cell classes are flexible entities. Nat Rev Neurosci 5:121–134.
Surwillo WW (1961) Frequency of the "alpha" rhythm, reaction time and age. Nature 191:823–824.
Tai C, Kuzmiski JB, MacVicar BA (2006) Muscarinic enhancement of R-type calcium currents in hippocampal CA1 pyramidal neurons. J Neurosci 26:6249–6258.
Traub RD, Bibbig A (2000) A model of high-frequency ripples in the hippocampus based on synaptic coupling plus axon-axon gap junctions between pyramidal neurons. J Neurosci 20:2086–2093.
Traub RD, Bibbig A, LeBeau FE, Cunningham MO, Whittington MA (2005) Persistent gamma oscillations in superficial layers of rat auditory neocortex: experiment and model. J Physiol (Lond) 562:3–8.
Turner JP, Anderson CM, Williams SR, Crunelli V (1997) Morphology and membrane properties of neurones in the cat ventrobasal thalamus in vitro. J Physiol (Lond) 505:707–726.
VanRullen R, Koch C (2003) Is perception discrete or continuous? Trends Cogn Sci 7:207–213.
Varela FJ, Toro A, John ER, Scwartz EL (1981) Perceptual framing and cortical alpha rhythm. Neuropsychologia 19:675–686.
Zhan XJ, Cox CL, Sherman SM (2000) Dendritic depolarization efficiently attenuates low-threshold calcium spikes in thalamic relay cells. J Neurosci 20:3909–3914.
Zhu JJ, Uhlrich DJ (1998) Cellular mechanisms underlying two muscarinic receptor-mediated depolarizing responses in relay cells of the rat lateral geniculate nucleus. Neuroscience 87:767–781.
Zhu L, Blethyn KL, Cope DW, Tsomaia V, Crunelli V, Hughes SW (2006) Nucleus- and species-specific properties of the slow (<1 Hz) sleep oscillation in thalamocortical neurons. Neuroscience 141:621–636.